ORNL/TM-6414

Irradiation Performance of HTGR Biso Fertile Particles in HFIR Experiments HT-17, -18, and -19

E. L. Long, Jr.
R. L. Beatty
J M Robbins
M. J. Kania
W. P. Eatherly

OAK RIDGE NATIONAL LABORATORY
OPERATED BY UNION CARBIDE CORPORATION · FOR THE DEPARTMENT OF ENERGY

DISCLAIMER

Printed in the United States of America. Available from
National Technical Information Service
U.S. Department of Commerce
5285 Port Royal Road, Springfield, Virginia 22161
Price: Printed Copy $4.50; Microfiche $3.00

ORNL/TM-6414
Dist. Category UC-77

Contract No. W-7405-eng-26

Metals and Ceramics Division

HTGR Base Technology Program

Fueled Graphite Development (189a 01330)

IRRADIATION PERFORMANCE OF HTGR BISO FERTILE PARTICLES IN HFIR EXPERIMENTS HT-17, -18, AND -19

E. L. Long, Jr. R. L. Beatty J M Robbins
M. J. Kania W. P. Eatherly

DATE PUBLISHED: NOVEMBER 1978

Prepared by the
OAK RIDGE NATIONAL LABORATORY
Oak Ridge, Tennessee 37830
operated by
UNION CARBIDE CORPORATION
for the
DEPARTMENT OF ENERGY

THIS PAGE

WAS INTENTIONALLY

LEFT BLANK

CONTENTS

IRRADIATION PERFORMANCE OF HTGR BISO FERTILE PARTICLES IN HFIR EXPERIMENTS HT-17, -18, and -19

E. L. Long, Jr. R. L. Beatty J M Robbins
M. J. Kania W. P. Eatherly

ABSTRACT

A series of Biso-coated fertile particles were irradiated in the target facility of the High-Flux Isotope Reactor. The primary objectives of this experiment were to relate the fast-neutron stability of dense propylene-derived pyrocarbons to preferred orientation and to relate irradiation performance to preirradiation characterization values. Coating characterization included x-ray BAF, optical anisotropy, gaseous permeability, small-angle x-ray scattering, and thickness and density determinations. Other objectives were to test Biso-coated large-diameter ThO_2 kernels and coatings derived from propylene diluted with CO_2 rather than argon.

Visual examination of the irradiated particles showed that the majority had failed as a result of fast-neutron damage. Some correlation could be made of particle failures with preirradiation optical anisotropy values. But the most consistent correlation was with small-angle x-ray scattering data. The performance of the coating prepared from CO_2-diluted propylene was outstanding; no failures were observed after the HTGR-design fast fluence was exceeded by 75% at a maximum particle surface temperature of 1575°C.

INTRODUCTION

Irradiation test capsules HT-17, -18, and -19 were part of a continuing series of experiments designed to test Biso coatings on thoria kernels. The static, sealed capsules were irradiated for two, four, and six cycles, respectively, in the target facility of the High Flux Isotope Reactor (HFIR). The three capsules were shared by ORNL and General Atomic Company (GA), but this report will address only the results from the ORNL portion of the experiment. The GA experiment has been reported separately.[1] The ORNL test specimens were Biso-coated fertile particles having nominal 500- and 700-μm sol-gel thoria kernels.

The experimental format resembled that of HT-12 through -15 (ref. 2) in that the test samples were loose, coated particles contained in small annular graphite holders stacked in graphite sleeves. Each capsule was designed to test particles at graphite holder surface temperatures of 900 and 1250°C and to burnup and fast-neutron exposures of at least one and a half times the HTGR design values. These surface temperatures correspond to particle temperatures of about 1200 and 1500°C, respectively.

The major objective of the ORNL experiment was to define the fast-neutron irradiation stability of the dense pyrocarbon coatings as a function of preferred orientation. Derived from propylene, all the dense pyrocarbons were deposited so that the concentration varied to produce a range of preferred orientations (anisotropies) of the coatings. Anisotropies were measured both optically (OPTAF) and by an x-ray technique (BAF). The BAF (Bacon Anisotropy Factor) measurements were made on flat strips of coatings deposited on graphite plates fluidized with the particles.

Two secondary objectives were to test a large thoria kernel (nominally 700 μm) with a proportionately scaled Biso coating and a dense pyrocarbon coating deposited from propylene diluted with CO_2 rather than the usual argon.

PREPARATION AND CHARACTERIZATION OF COATED PARTICLES

For all batches except one, the nominal particle dimensions were: a 500-μm kernel diameter, a 75-μm buffer, and an 80-μm dense outer coating. A peripheral experiment used one batch of thoria kernels with a 680-μm diameter and a proportionately scaled Biso coating. All the 500-μm kernels were buffer coated in a 0.13-m coater as a single batch to prevent variations in the buffer coating. All other coatings were deposited by a 0.025-m laboratory-scale coater. The dense outer coatings were deposited from propylene; the primary process variable being propylene concentration and hence, deposition rate. This effectively varies the coating anisotropy. During each outer coating run several graphite plates were included in the batch to obtain specimens for x-ray BAF measurements. The coating deposition conditions, thicknesses, and densities are listed in Table 1.

Table 1. Deposition conditions and property measurements of ORNL particles from experiments HT-17, -18, and -19

Batch[a]	Deposition conditions[b]			Deposition rate[b] (μm/s)	Measured properties					
					Buffer			Outer coating		
	Temperature (°C)	Propylene flux ($m^3/s \cdot m^2$)	Propylene concentration[c] (%)		Mean thickness[d] (μm)		Mean density[e] (Mg/m^3)	Mean thickness[d] (μm)		Mean density[d] (Mg/m^3)
OR-1975-T	1315	6.66	33.3	70.8	68.5	(7.8)	1.19	83.0 (3.5)		1.982 (0.007)
OR-1967-T	1300	3.33	16.7	31.2	75.6	(5.2)	1.19	78.4 (3.7)		2.000 (0.007)
OR-1986-T	1250	1.83	9.2	12.6	69.2	(7.2)	1.19	78.6 (3.5)		2.102 (0.010)
OR-1985-T	1275	2.08	10.4	17.4	71.0	(7.6)	1.19	76.4 (3.9)		2.065 (0.008)
OR-1987-T	1250	1.50	7.5	10.2	72.4	(9.8)	1.19	84.9 (4.3)		2.094 (0.005)
OR-1972-T	1250	1.66	8.4	12.0	69.4	(6.2)	1.19	78.7 (4.3)		2.063 (0.009)
OR-1978-T	1240	0.83	4.2	4.8	69.8	(4.1)	1.19	83.9 (3.6)		2.072 (0.005)
OR-2012-ST	1200-1350[f]	2.50	12.5	22.2	74.1	(6.3)	1.19	100.4 (3.0)		1.919 (0.009)
OR-2013-T	1325	6.66	33.3	69.0	80.4	(6.9)	1.19	84.5 (3.9)		2.002 (0.009)
OR-2010-T	1335	15.0	33.3	135.0	96.6	(8.6)	1.08	105.4 (5.4)		1.980 (0.009)

[a] Kernels 500 μm in diameter, except OR-2010-T, which are nominally 700 μm in diameter.

[b] Outer coating only; buffer coating deposited from acetylene.

[c] Diluted with argon, except OR-2013-T, which was diluted with CO_2.

[d] Numbers in parentheses are standard deviations.

[e] Calculated, includes seal coating.

[f] Temperature increased 6°C/min during run to produce radial property gradients.

In addition to the primary specimen set in which the outer coating deposition rate (propylene concentration with argon diluent) was varied, three specimens were included for peripheral experiments. These experiments, respectively, used the large particles mentioned above (OR-2010-T), a coating deposited at gradually increasing temperatures (OR-2012-ST), and a coating deposited with CO_2 rather than argon diluent as the fluidizing gas (OR-2013-T). The large particles were included to determine whether or not the standard 500-μm-diam thoria approached an upper size limit for satisfactory coating performance. The large particle was omitted from the high-temperature section of the six-cycle HT-19 test because the ^{233}U buildup late in the test would have raised the power generation per particle and hence, the internal particle temperature to unrealistically high levels. The coating deposited at variable temperatures was fabricated with a temperature rise programmed to simulate a possible production furnace run. Since coating density is strongly a function of deposition temperature, this procedure should result in a significant radial density gradient. Unfortunately, no technique currently exists to measure the gradient, so the density reported is an average value. The coating deposited with CO_2 diluent gas was included to test a process developed earlier. The test showed that oxidizing fluidizing gases can be employed up to certain limits in pyrocarbon coating to reduce soot deposition in the coating chamber without harming coating properties.[3]

The coating set listed in Table 1 was intended to bracket the survival-failure line at various fluences in correlation with deposition rate and BAF. The maximum BAF value a coating may have to survive a given fluence is not well defined. However, we thought that deposition rates exceeding 5 μm/min would produce coatings able to survive the HTGR design fluence (≈4 HT cycles at the HFIR midplane).

BAF Measurements

A set of BAF standards was prepared, as were coated particles for irradiation experiments HT-17 through HT-19. Since the purpose of these tests was to compare coatings of varied anisotropies, the coating runs conveniently allowed us to fabricate the required set of flat plate

specimens. The anisotropy specimens in this case were deposited onto graphite plates 7.9 mm square by 0.76 mm thick, fluidized along with the particles. The coatings were removed from the graphite substrate as 5.1 mm-square plates and x-rayed.

Each plate was placed in a collimated x-ray beam with the plane of deposition at 13° (the Bragg angle for the first-order basal reflection) to the beam. This produced a diffraction ring with radial integrated intensity proportional at given angular positions to the number of crystallites with basal planes aligned parallel to the corresponding angle in the specimen. Absorption corrections had to be made to maintain the proportionality over the full 0 to 90° span, but absorptions at the 0 and 90° positions are nearly identical. Thus, for convenience and accuracy a BAF analytical technique developed by Tassone[4] was applied to the 0 and 90° relative intensities; it required no significant corrections. The x-ray films were scanned with an optical microdensitometer at the 0 and 90° positions and BAF values were obtained from the ratio of integrated intensities. Measurements on the HT-17 through HT-19 specimens showed BAF values (listed in Table 2) ranging from 1.00 to 1.73.

Optical Anisotropy Measurements

While the x-ray (BAF) method — requiring flat strip specimens — has been applied extensively to fluidized-bed pyrolytic carbons, the optical (OPTAF) method is favored because it can directly monitor anisotropy in microsphere coatings. In addition, OPTAF is preferable because it does not require the tedious preparation — by coating — of flat specimens with each batch of microspheres; and hence, it avoids the uncertainty about the degree to which the plate coating represents the microsphere coating. However, the OPTAF measurements must be calibrated against x-ray BAF determinations if results are to be correlated with data and experience.

A series of optical anisotropy measurements (OPTAF) were made on the LTI coatings selected for irradiation in HT-17, -18, and -19. At the time these measurements were made the OPTAF equipment at ORNL was

under development,[5] but because superior OPTAF equipment was developed at GA, operation of this equipment has since been discontinued. Samples from five batches were selected for OPTAF measurements at ORNL. We believe the samples covered the range of anisotropies, based on x-ray BAF measurements. Samples of particles from four of these five were measured at KFA* Jülich, Federal Republic of Germany, and two were measured at GA for comparison with the ORNL measurements. Samples of particles from all the batches used in this experiment were measured at ÖSGAE,† Seibersdorf, Austria. The results of these measurements are listed in Table 2. Although the measurements varied somewhat, the particles with the lowest OPTAF values — determined by all four facilities — were from batch OR-2013-T, the batch prepared from CO_2-diluted propylene.

Permeability Measurements

The Biso coating design requires the pyrocarbon coating to serve as a pressure vessel to retain gaseous fission products; thus, both permeability and strength of the coating are important. Permeability can be measured by measuring the intrusion of low-atomic-number inert gases such as neon and helium through Biso coatings. The method consists of determining the ratio of neon to helium (Ne/He) in the particle void space after heating to 1375°C for 1 hr in an atmosphere of equal parts of neon and helium.[6] After heat treatment the particles are individually broken in a chamber connected to a mass spectrometer. The amount of gas retained is determined for each particle in a set of 15 and the results are averaged. The procedure requires 1 to 2 min per fuel particle for a measurement. The Ne/He ratio in the retained gas is a good relative measure of the pyrocarbon coating permeability for Biso particle batches that have roughly equal ratios of surface area to void volume in the buffer layer. For coated particles having a significantly different ratio of surface area to void volume, dimensionally based adjustments must be made to obtain comparable Ne/He ratios. The Ne/He ratios determined for the Biso

*Kernforschungsanlange.

†Österreichische Studiengesellschaft für Atomenergie.

particles in the experiment are listed in Table 2. The Ne/He intrusion values ranged between 0.03 and 0.19, which indicates low-permeability coatings. The trend of increasing permeability with increasing coating rate is shown in Fig. 1.

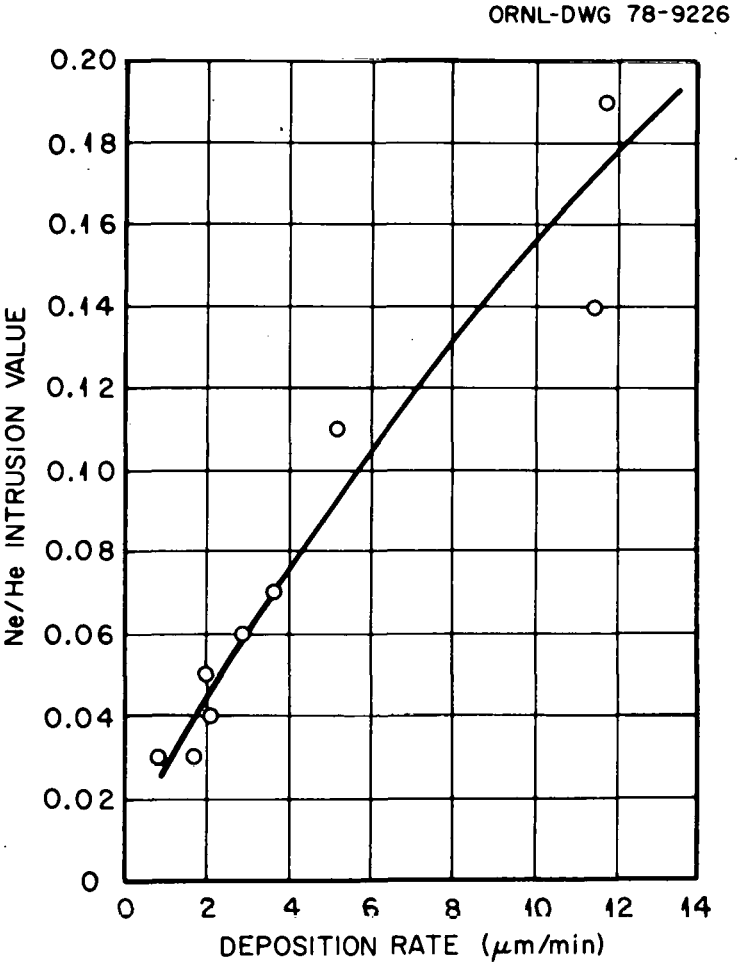

Fig. 1. Ne/He intrusion ratio as a function of coating rate for Biso particles irradiated in HT-17, -18, and -19.

Small-Angle X-Ray Scattering Measurements

Small-angle x-ray scattering (SAXS) was used to characterize the microstructure of the LTI coatings. The distribution of microporosity within the coatings can be determined from SAXS measurements, which have been correlated with the microstructural components of pyrocarbon.[7] A

parametric property, relative amount of fiber component (RAF),* has been developed and correlated with the relative concentrations of micropores ranging in size from 6 to 25 nm. This property, RAF, has been correlated with deposition conditions, physical properties, and irradiation behavior of other coatings.[8] The RAF values for the LTI coatings irradiated in HT-17, -18, and -19 are listed in Table 2. The correlation of increasing RAF values with increasing deposition rate and temperature for the particles containing the nominal 500-μm-diam kernels is shown in Fig. 2. Correlating RAF with the values of Ne-to-He intrusion ratios, Fig. 3, shows a proportional relationship to exist between these two properties.

*RAF (relative amount of fiber component) is calculated as follows:

$$RAF = \frac{2C_{10} + C_{20}}{3}$$

where

C_{10} = Relative concentration of pores in a size range of 6 to 12 nm.

C_{20} = Relative concentration of pores in a size range of 12.1 to 25 nm.

Table 2. Results from OPTAF, BAF, Ne/He, and RAF measurements on coatings irradiated in HT-17, -18, and -19

Batch	Bacon anisotropy factor (optical) (BAF)				Bacon anisotropy factor (x-ray) (BAF) (ORNL)	Ratio of Ne to He (ORNL)	Relative amount of fiber component (RAF) (KFA)
	(ORNL)	(KFA)	(ÖSGAE)	(GA)			
OR-1978-T	1.51	ND[a]	1.380	1.44	1.73	0.03	0.59
OR-1987-T	ND	ND	1.148	ND	1.17	0.03	ND
OR-1972-T	ND	ND	1.083	ND	1.22	0.05	0.74
OR-1986-T	ND	ND	1.138	ND	1.10	0.04	ND
OR-1985-T	1.03	1.026	1.065	ND	1.12	0.06	0.79
OR-1967-T	1.02	1.014	1.045	ND	1.05	0.11	0.93
OR-2013-T	1.02	1.014	1.028	1.02	1.00[b]	0.14	1.03
OR-1975-T	1.02	1.029	1.063	ND	1.00	0.19	0.97
OR-2012-ST	ND	ND	1.078	ND	gradient	0.07	ND
OR-2010-T	ND	ND	1.013	ND	1.00[b]	ND	0.79

[a]Not determined.

[b]Estimated from coating run conditions.

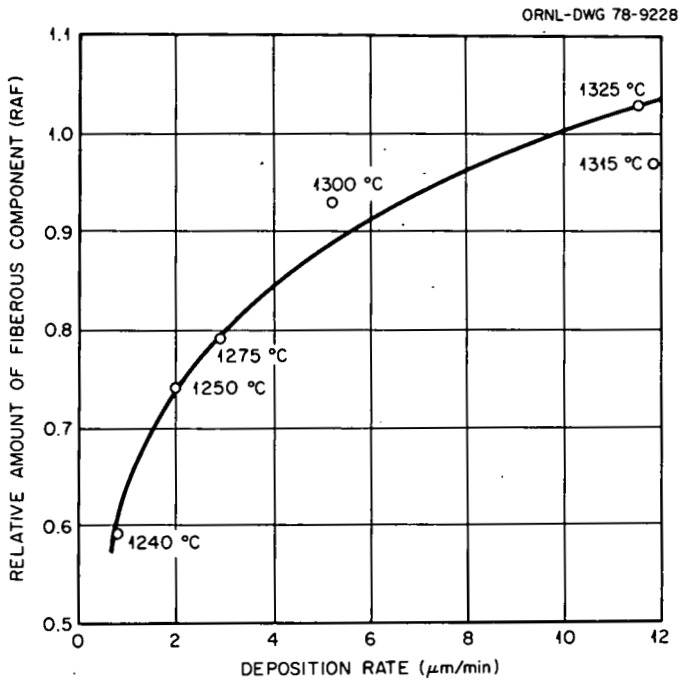

Fig. 2. Correlation of relative amount of fibrous component with coating rate for the LTI coatings irradiated in HT-17, -18, and -19. Deposition temperatures in degrees Centigrade are indicated by each datum point.

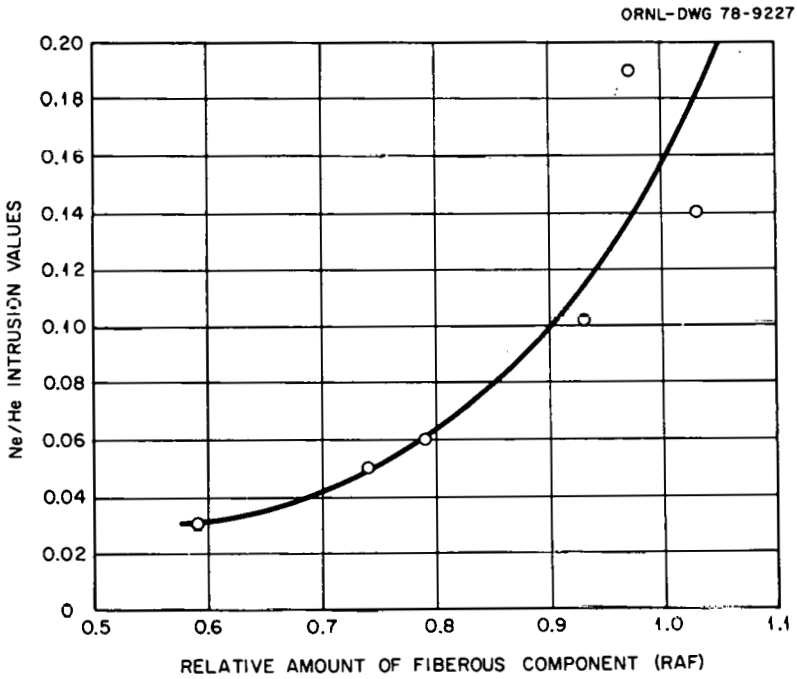

Fig. 3. Correlation of relative amount of fibrous component with relative gaseous permeability of LTI coatings irradiated in HT-17, -18, and -19.

CAPSULE DESIGN

Capsules HT-17, -18, and -19 were similar in design to HFIR target tests HT-12 through -15 (refs. 9, 10). The capsules, as shown in Fig. 4, were made of aluminum, were uninstrumented, and were backfilled with argon. Each capsule had the following design features:

- four graphite magazines, two designed for a nominal particle holder surface temperature of 900 and 1250°C;
- a total of 32 test holders for fertile particles, eight in each magazine;
- two samples of each test specimen type, one in each temperature zone;
- a total of 0.905 g Th, 0.530 g in the high-temperature zone and 0.375 g in the low-temperature zone;
- a porous carbon heat shield separating the two temperature zones; and
- a total of 0.459 g U, 6.5% enriched ^{235}U, 0.268 g of the total in the high-temperature zone and 0.191 g in the low-temperature zone. The uranium was present as SiC-coated weak-acid resin particles distributed equally in five particle holders and one end plug in each magazine to smooth out heat generation curves and maintain the temperature as nearly constant as possible throughout the irradiation.

The loading arrangement for the ORNL fertile test particles is shown in Table 3. After each coating step the particles were sized to minimize extraneous results that might be introduced by dimensional variations. After the buffer and sealers were applied, the particles were also sized on a roller micrometer to eliminate excessively thick or thin coatings. After all coatings were applied, the particles were again sized on a roller micrometer. The sized fraction of the particles with 500-μm-diam kernels was poured over an x-ray holder with 144 holes that captured one particle in each hole. From the radiograph of these

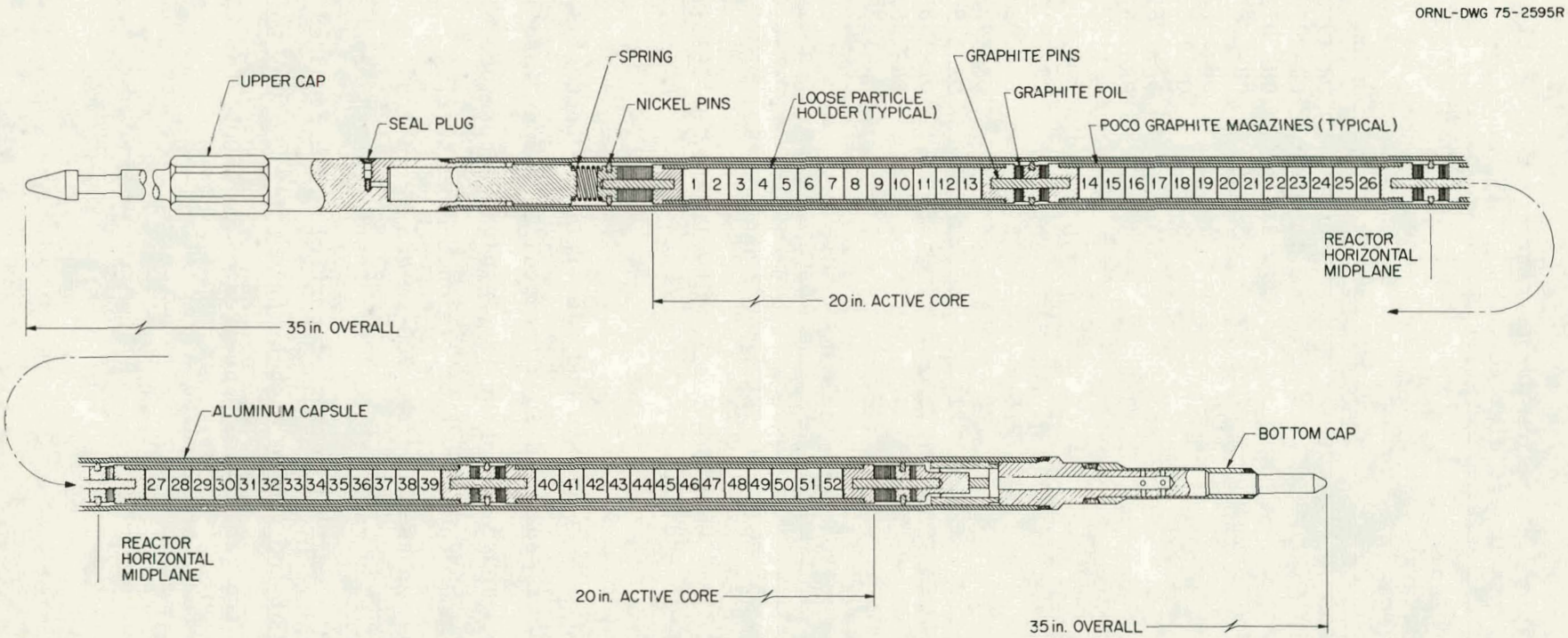

Fig. 4. Target capsule design typical of HT-17, -18, and -19.

Table 3. Loading arrangement for ORNL fertile test particles for HT-17, -18, and -19

Design Temperature (°C)	Sample holder	Item	Batch
900	2	7	OR-1978-T
	4	10	OR-2010-T
	5	8	OR-2012-ST
	7	5	OR-1987-T
	8	6	OR-1972-T
	10	3	OR-1986-T
	11	4	OR-1985-T
	13	2	OR-1967-T
1250	15	10[a]	OR-2010-T
	17	8	OR-2012-ST
	18	5	OR-1987-T
	20	6	OR-1972-T
	21	3	OR-1986-T
	23	4	OR-1985-T
	24	2	OR-1967-T
	26	7[b]	OR-1978-T
Reactor midplane			

[a]This particle replaced by item 1, OR-1975-T in HT-19.

[b]This particle replaced by item 9, OR-2013-T in HT-18 and -19.

144 particles, 99 were chosen and identified to be tested. The 99 particles were separated in a nonspecific manner into samples of 58 and 41 particles for testing in the high-temperature high-flux region and the low-temperature low-flux region, respectively. A similar selection technique was used for the 700-μm-diam kernel batch, except only 22 and 16 particles were selected for testing in the two temperature-flux zones. The smaller number of particles was required because of the larger amount of thorium in each kernel.

All graphite parts were heat-treated to 1500°C for 30 min in an argon atmosphere before loading.

IRRADIATION HISTORY

Capsule HT-17 was inserted in target position A-3 on July 22, 1973, and was removed on Sept. 8, 1973, after 46.42 days (two HFIR cycles) at 100 MW reactor power. The peak fast fluence was 4.73×10^{25} neutrons/m^2 ($E > 0.18$ MeV) and the peak fertile particle burnup was 2.88% FIMA.

Capsule HT-18 was inserted in target position E-2 on July 22, 1973, and was removed on Oct. 28, 1973, after 92.94 days (four HFIR cycles) at 100 MW reactor power. The peak fast fluence was 9.48×10^{25} neutrons/m^2 ($E > 0.18$ MeV) and the peak fertile particle burnup was 9.7% FIMA.

Capsule HT-19 was inserted in target position F-7 on July 22, 1973, and was removed on Dec. 17, 1973, after 139.27 days (six HFIR cycles) at 100 MW reactor power. The peak fast fluence was 1.4×10^{26} neutrons/m^2 ($E > 0.18$ MeV) and the peak fertile particle burnup was 17.24% FIMA. Table 4 gives the fast fluence and burnup for each fertile particle specimen in each capsule. No attempt was made to calculate the fissile particle burnup. Table 5 gives the operating history of the reactor during the irradiation of each capsule.

THERMAL ANALYSIS

Since there are no provisions for direct temperature monitoring or for a sweep gas system in the HT capsules, thermal modeling is used to predict maximum fuel operating temperatures. For capsules HT-17 through 19 the thermal modeling code HTCAP was used to determine the maximum operating temperatures for each ThO_2 particle in each of the capsules.[10] Maximum particle surface operating temperatures were calculated at two-day intervals for each HFIR irradiation cycle.

Temperature calculations were based on knowledge of the dimensional change characteristics of the graphite sample holders, graphite magazines, and aluminum containment vessel as a function of temperature and fast-neutron fluence ($E > 0.18$ MeV); fission heat generated per particle based on isotopic density changes as a function of time; gamma heating rates; changes in material thermal conductivities as a function of temperature and fast-neutron fluence ($E > 0.18$ MeV); and the coolant temperature at

Table 4. Fast-neutron flux, fast-neutron fluence, and burnup for specimens in HFIR target capsules HT-17, -18, and -19

Sample holder	Fast-neutron fluence, neutrons/m^2 (E > 0.18 MeV)			Fast-neutron flux, neutrons/m^2s (E > 0.18 MeV)	Distance from holder center to reactor midplane (mm)	Fertile particle burnup, % FIMA		
	HT-17	HT-18	HT-19			HT-17	HT-18	HT-19
1,52	2.24×10^{25}	4.51×10^{25}	6.75×10^{26}	0.56×10^{19}	233.7			
2,51	2.37	4.74	7.10	0.59	226.3	1.40	5.25	9.91
3,50	2.54	5.09	7.63	0.63	219.1			
4,49	2.72	5.44	8.15	0.67	211.9	1.57	5.78	10.83
5,48	2.83	5.68	8.50	0.70	204.7	1.63	6.05	11.30
6,47	2.95	5.91	8.85	0.73	197.6			
7,46	3.07	6.14	9.20	0.76	190.4	1.81	6.53	12.10
8,45	3.21	6.44	9.64	0.80	183.2	1.90	6.78	12.52
9,44	3.30	6.61	9.90	0.82	176.0			
10,43	3.42	6.85	10.3	0.85	168.9	2.03	7.20	13.25
11,42	3.56	7.14	10.7	0.88	161.7	2.10	7.43	13.60
12,41	3.68	7.37	11.0	0.91	154.5			
13,40	3.74	7.49	11.2	0.93	147.3	2.22	7.82	14.21
14,39	4.23	8.49	12.7	1.05	106.7			
15,38	4.26	8.54	12.8	1.06	99.3	2.61	8.88	15.88
16,37	4.35	8.72	13.1	1.08	92.1			
17,36	4.41	8.84	13.2	1.09	84.9	2.70	9.11	16.27
18,35	4.47	8.95	13.4	1.11	77.7	2.72	9.22	16.43
19,34	4.53	9.07	13.6	1.12	70.6			
20,33	4.55	9.13	13.7	1.13	63.4	2.80	9.40	16.71
21,32	4.58	9.19	13.8	1.14	55.2	2.81	9.48	16.85
22,31	4.64	9.30	13.9	1.15	48.0			
23,30	4.67	9.36	14.0	1.16	41.9	2.85	9.60	17.03
24,29	4.70	9.42	14.1	1.16	34.7	2.87	9.64	17.12
25,28	4.73	9.48	14.2	1.17	27.5			
26,27	4.73	9.48	14.2	1.17	20.3	2.88	9.70	17.24

Table 5. Operational history of capsules HT-17 through -19

HFIR cycle	Dates		Length of operation (d)	Accumulated irradiation time at 100 MW reactor power (d)
	Cycle beginning	Cycle end		
		Capsule HT-17		
95	7/22/73	8/15/73	23	23.20
96	8/16/73	9/8/73	23	46.42
		Capsule HT-18		
95	7/22/73	8/15/73	23	23.20
96	8/16/73	9/8/73	23	46.42
97A[a]	9/9/73	9/17/73		
97B	9/17/73	10/5/73	26	69.58
98	10/5/73	10/28/73	23	92.94
		Capsule HT-19		
95	7/22/73	8/15/73	23	23.20
96	8/16/73	9/8/73	23	46.42
97A[a]	9/9/73	9/17/73		
97B	9/17/73	10/5/73	26	69.58
98	10/5/73	10/28/73	23	92.94
99	10/31/73	11/23/73	23	116.23
100	11/25/73	12/17/73	23	139.27

[a]Reactor began a programmed reduction in power on 9/14/73 in preparation for the shutdown on 9/17/73.

the containment surface. A detailed description of the calculational procedure is described in reference 11.

The dimensional change data for capsules HT-17 through -19 were limited in that postirradiation dimensional data were obtained only on capsule HT-19. The results of these measurements, as well as the preirradiation design dimensions, are shown in Appendix A, Tables A-1 and A-2, for the graphite magazines and graphite crucibles, respectively. These data and the postirradiation dimensional data from graphite components from capsules HT-14 and -15 were used as supplemental data for HT-17 and -18 and incorporated into the HTCAP code.

A significant portion of the heat generated in an HT capsule is from gamma heating of the capsule components. Figure 5 describes the gamma heating rate[12] for graphite in the HFIR target region as a function of distance from the horizontal midplane (HMP) of the reactor. This same function was used for the gamma heating rate for the aluminum.

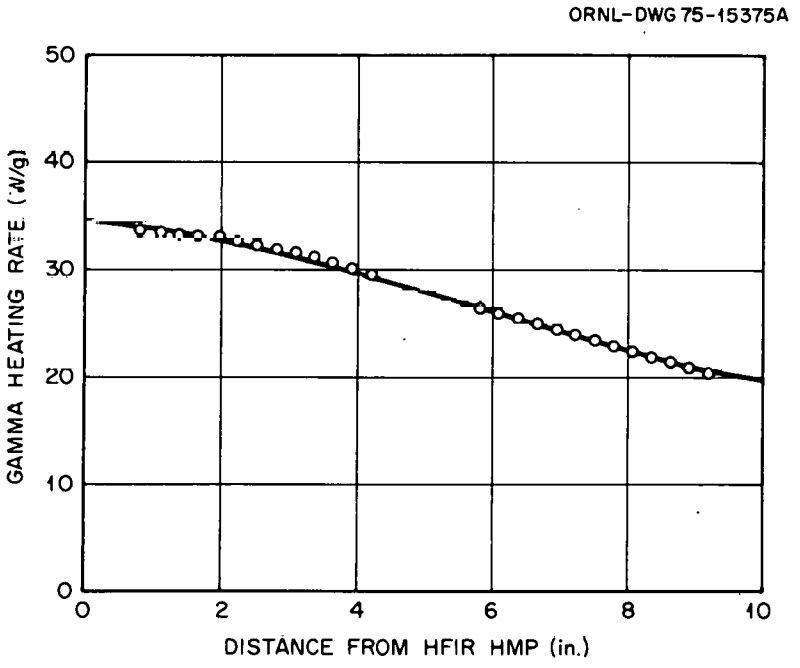

Fig. 5. Gamma heating rate for graphite in the HFIR target facility as a function of axial distance from the reactor horizontal midplane. To convert to millimeters multiply by 25.4.

The design operating temperatures for the outer surface of the particle holders in capsules HT-17 through -19 were 900°C for the low-temperature magazine and 1250°C for the high-temperature magazine. Operating temperature histories derived from the HTCAP code for each Biso ThO_2 particle irradiated are shown in Appendix B, Figs. B.1 and B.2. For each particle type the maximum particle surface temperature, graphite annulus temperature (holder temperature), and power generated per particle are described as a function of irradiation time.

The following conclusions can be drawn from these data:

1. Graphite holder operating temperatures were 50 to 100°C higher than the design temperature of 900°C for the low-temperature magazine.

In the high-temperature magazine the graphite holders operated at 50 to 150°C higher than the design temperature of 1250°C. The temperature increase depended on holder position with respect to the reactor horizontal midplane.

2. Maximum particle surface temperatures were 300 to 400°C higher than were holder temperatures in the low-temperature magazine. Particle type OR-2010-T, with a 1083-μm diameter, had the highest temperature difference. In the high-temperature magazine, the maximum particle surface temperatures were 200 to 250°C higher than holder temperatures were. Peak particle surface temperatures occurred at the end of the sixth cycle (HT-19) in the low-temperature magazine and during the fourth cycle (HT-18) in the high-temperature magazine.

3. Average particle operating temperatures for capsules HT-18 and -19 were determined to range from 1250 to 1350°C for the low-temperature magazine and from 1550 to 1650°C in the high-temperature magazine.

POSTIRRADIATION EXAMINATION

The capsules were transferred from HFIR to the High-Radiation Examination Laboratory (HRLEL) for disassembly and examination. The graphite magazines appeared free of soot; this was attributed to the gettering action of zirconium foil disks between particle holders in each magazine. The graphite holders from HT-17 and the low-temperature region of HT-18 were easily removed. However, the magazines in HT-19 and the high-temperature magazine of HT-18 had to be slit open to recover the graphite holders. The holders from the higher temperature magazine of HT-18 and -19 were quite fragile and had to be broken to recover the particles. The tops of the other holders unscrewed easily. The results of the visual examinations, made with the aid of a shielded stereomicroscope, are listed in Table 6. Two failure mechanisms were identified: failures that resulted from fast-neutron damage to the coatings and pressure-vessel failures. Examples of these failure mechanisms are shown in Fig. 6. Pressure-vessel failure causes the coatings to fragment, while fast-neutron damage causes them to unfold. As Table 6 shows, most coating failures occurred at low fluences and were fast-neutron induced.

Table 6. Percent failures and failure mechanisms for Bisc fertile particles irradiated in HT-17, -18, and -19

Batch	HT-17 (2 cycles)				HT-18 (4 cycles)				HT-19 (6 cycles)			
	Failures, %		Mechanism[a]		Failures, %		Mechanism[a]		Failures, %		Mechanism[a]	
	Low[b]	High[c]	Low[b]	High[c]	Low[b]	High[c]	Low[b]	High[c]	Low[b]	High[c]	Low[b]	High[c]
OR-1967-T	0	100		FND	100	100	FND	*d*	98	100	FND	FND
OR-1985-T	7	100	PV	PV	100	100	FND	*d*	100	100	FND	*d*
OR-1986-T	76	0	FND		100	100	FND	FND	100	100	FND	FND
OR-1972-T	0	100		PV	100	100	FND	FND	92	100	FND	*d*
OR-1987-T	0	100		FND	100	100	FND	FND	100	100	FND	*d*
OR-1978-T	0	100		FND	100	NI	FND		100	NI	FND	
OR-2013-T[e]	NI[f]	NI			NI	0			NI	0		
OR-1975-T	NI	NI			NI	NI			NI	91		FND
OR-2010-T[g]	0	0			0	14		PV	6	NI	PV	
OR-2012-ST[h]	0	16		PV	100	100	FND	FND	100	100	FND	*d*

[a] Pressure Vessel.

Fast-Neutron Damage.

[b] Irradiated in low-temperature magazine.

[c] Irradiated in high-temperature magazine.

[d] Coating fragments and kernels either reacted or damage was too severe to identify failure mechanism.

[e] Coating deposited with a CO_2 diluent.

[f] Not Included in test.

[g] Nominal 700-μm-diam kernel.

[h] Radial density gradient coating.

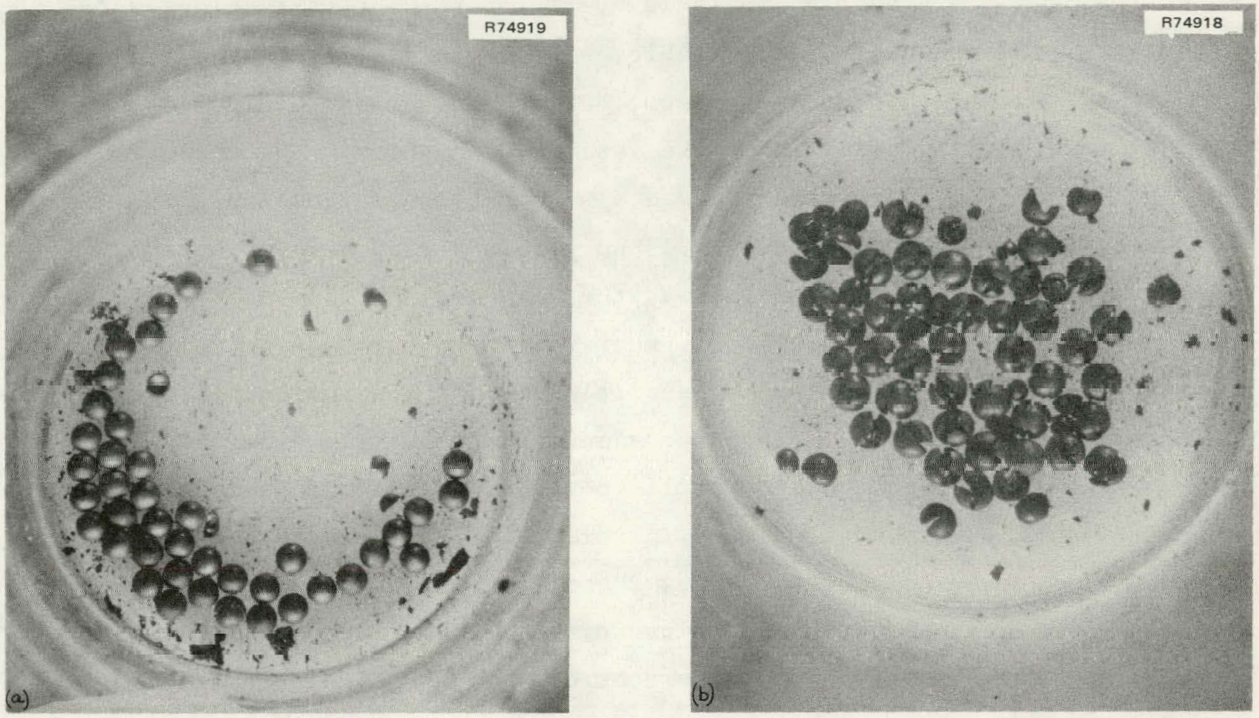

Fig. 6. Two failure mechanisms observed during the postirradiation examination of Biso particles from capsules HT-17 through -19. (a) Pressure-vessel failures of OR-1985-T from the low-temperature region of HT-17. (b) Failures resulting from fast-neutron damage to the coatings of OR-2012-ST from the low-temperature region of HT-18.

DISCUSSION OF RESULTS

Although most coating failures resulted from fast-neutron damage, a statistical analysis was performed to identify any coating that might have improper thickness, which could lead to pressure-vessel failure. Despite the fact that the particles were sized with a roller micrometer after the buffer and sealer coats had been applied, considerable variability of the buffer coating thicknesses was observed in radiographs of the final heat-treated coated particles. This was surprising in that the individual particle batches were all derived from the same seal-coat run (A-242) and buffer run (A-240) performed in a 0.13-m coater.

The data are presented in Table 7. The pertinent statistical variable is k, the non-central t variable, here calculated against a minimum acceptable buffer thickness of 52 μm, 80% of the nominal minimum 65-μm buffer desired. An analysis of the variances of the nine batches with presumably identical buffers yielded a within-batch variance of 6.98 μm and a between-batch variance of 2.15 μm. This latter value is just significantly different from zero at the 95% confidence level. Moreover, neither the batch means nor their variances form any pattern in contrast to those of the coating conditions. The conclusion is that all buffer coatings are in fact the same, and the sample size of 25 particles per batch was too small to reliably estimate the distribution tails. Hence, differences in failure of the irradiated particles cannot be attributed to differences in buffer coatings.

The geometrical characteristics of the LTI coatings are given in Table 8. Again, the k values vary considerably as calculated against a minimum acceptable thickness of 67.5 μm, 90% of the nominal minimum

Table 7. Statistical analysis of buffer coatings on particles for HT-17 through -19

Batch	Description	Buffer thickness		Degrees of freedom	k
		Mean (μm)	Standard deviation (μm)		
A-240	Buffer only	86.86	9.73	24	
A-242	Buffer plus sealer	89.05	13.49	49	
A-242	Sized	77.98	7.99	24	
OR-1978-T	LTI coating rate 0.8 μm/min	69.84	4.10	24	4.35
OR-1987-T	1.7	72.43	9.75	24	2.10
OR-1972-T	2.0	69.37	6.23	24	2.79
OR-1986-T	2.1	69.23	7.24	24	2.38
OR-1985-T	2.9	71.03	7.60	24	2.50
OR-1967-T	5.2	75.64	5.23	24	4.52
OR-2013-T	11.5	71.68	8.69	24	2.26
OR-1975-T	11.8	68.51	7.84	24	2.11
OR-2012-ST	(3.7)	74.09	6.34	24	3.48
	Between batches		2.15	8	
	Within batches		6.98	216	
	Total	71.27	7.61	224	2.53

Table 8. Statistical analysis of pyrocarbon LTI coatings on particles for HT-17 through 19

Batch	LTI thickness,[a] μm		k
	Mean	Standard deviation	
OR-1978-T	83.9	3.6	4.556
OR-1987-T	84.9	4.3	4.046
OR-1972-T	78.7	4.3	2.605
OR-1986-T	78.6	3.5	3.171
OR-1985-T	76.4	3.9	2.282
OR-1967-T	78.4	3.7	2.946
OR-2013-T	84.5	3.9	4.359
OR-1975-T	83.0	3.5	4.428
OR-2012-ST	100.4	3.0	10.967

[a] 24 degrees of freedom for all analyses.

75-μm coating desired. Values of k as low as 2.28 permit 5.1% of the distribution to lie below 67.5 μm at the 95% level, and even a k of 3.17 leaves only 1.0% of the distribution below 67.5 μm. We may suspect that the mechanism of failure of batches OR-1985 and OR-1967 was pressure-vessel and, indeed, for OR-1985 after two HFIR cycles, it was. For those batches to have yielded k values of 4.0 would require standard deviations below 2.3 and 2.7 μm, respectively, well below any value expected from the laboratory coaters.

OPTAF (BAF_o) values for the above particle batches are summarized in Table 9. Also presented are the calculated surface temperatures of the particles; the fluence at which the particles, as visually examined, were still intact; and the fluences at which the failures were observed. The entry zero in the intact rows simply indicates the particles failed before reaching the lowest fluence level at which they were examined.

OPTAF (BAF_o) values determined by the various laboratories agree reasonably well, especially if one remembers that no attempt was generally made to measure the same particles or locations within coatings. The failure of batches with coating rates of 2.1 μm/min or less can be clearly ascribed to too much anisotropy.

Table 9. Anisotropy and failure data for particles in HT-17 through -19

Batch	Coating rate (μm/min)	OPTAF(BAF_o)				Low-temperature magazine[a]			High-temperature magazine[a]		
						Fluence, 10^{25} n/m^2		Temperature of coating (°C)	Fluence, 10^{25} n/m^2		Temperature of coating (°C)
		ORNL	KFA	ÖSGAE	GA	Particles still intact	Particle failure observed		Particles still intact	Particle failure observed	
OR-1978-T	0.8	1.51		1.380	1.44	2.37	4.74	1275	0	4.73	1525
OR-1987-T	1.7			1.148		3.07	6.14	1350	0	4.47	1550
OR-1972-T	2.0			1.083		3.21	6.44	1350	0	4.55	1550
OR-1986-T	2.1			1.138		0	3.42	1300	4.58	9.19	1550
OR-1985-T	2.9	1.03	1.026	1.065		0	3.56	1300	0	4.67	1575
OR-1967-T	5.2	1.02	1.014	1.045		3.74	7.49	1375	0	4.70	1550
OR-2013-T	11.5	1.02	1.014	1.028	1.02	Not tested		Not tested	14.2		1575
OR-1975-T	11.8	1.02	1.029	1.063		Not tested		Not tested		12.8	1500
OR-2012-ST	3.7[b]			1.078		2.83	5.68	1350	0	4.41	1500
OR-2010-T	22.5			1.013		2.72	8.15	1425	4.26	8.54	1650

[a] "0" indicates failure occurred before lowest fluence level at which they were examined.

[b] Average coating rate for gradient coating.

A more striking correlation of a measured property and irradiation performance can be made by comparing the coating RAF values with observed failures (Fig. 7). Failures occurred in all particle batches with RAF values less than 1.0. One sample of particles from OR-1985-T experienced a 7% failure rate at a fluence of 3.6×10^{25} neutrons/m^2 but showed 100% failure as the design fluence was approached. Two data points appear to depart from the pattern shown in Fig. 7; they are results from the high- and low-temperature magazines that contained the large-diameter ThO_2 particles (OR-2010-T) with significantly thicker coating layers than the standard Biso particles have. We note that although the anisotropy of the OR-2010-T coating was low (BAF_o = 1.013) and the failures were pressure-vessel failures, the RAF value was less than one, which indicated that the performance of the coatings was in question.

Also worthy of note was the outstanding performance of batch OR-2013-T. The gamma spectrum and gas content of these particles were measured after irradiation. The fission-product inventory for particles from HT-18

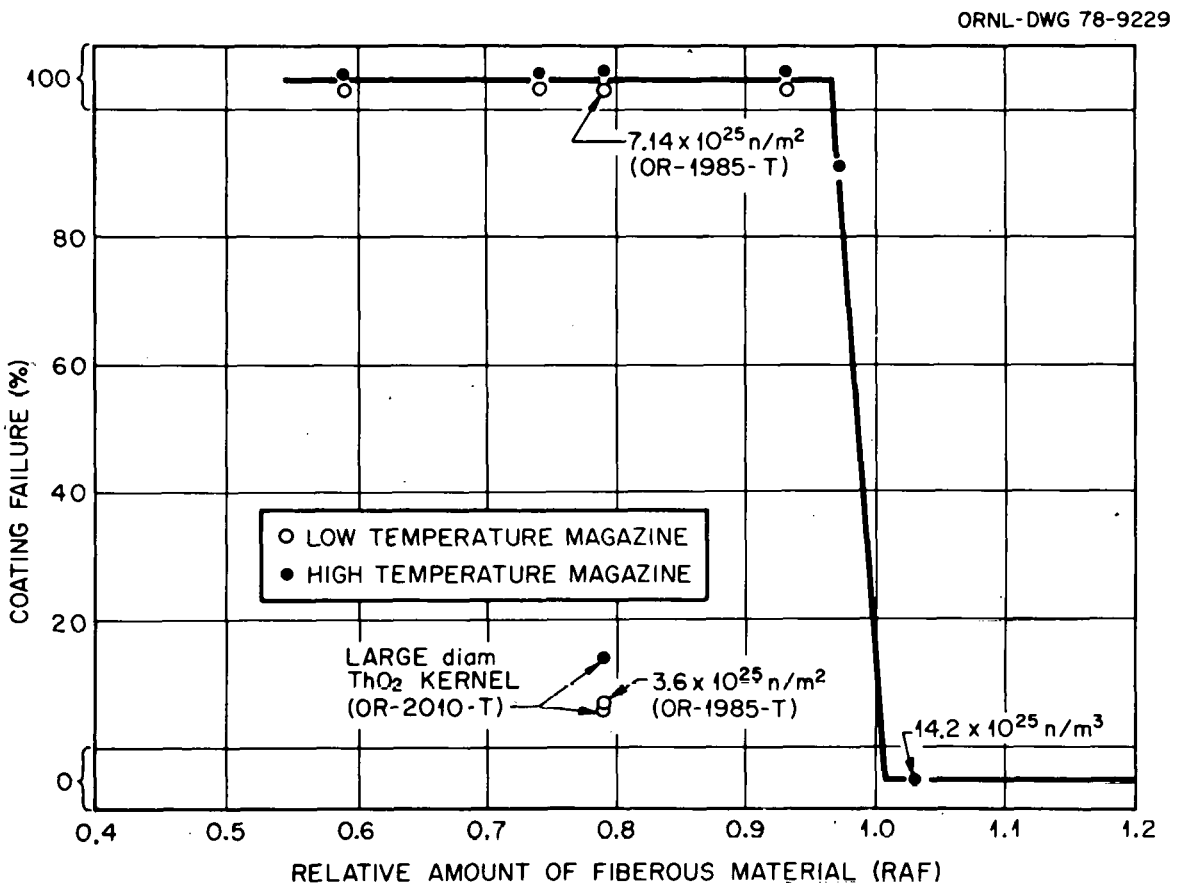

Fig. 7. Correlation of coating failures observed in HT-17, -18, and -19 with relative amount of fibrous material in the LTI layers.

(9.7% FIMA) showed that 24% of the ^{137}Cs was missing, while the expected amount of xenon, krypton, and carbon monoxide were present. The OR-2013-T particles from HT-19 (17.2% FIMA) showed a 28% loss of ^{137}Cs and again the expected carbon monoxide, krypton, and xenon contents. The ^{137}Cs loss was that anticipated for solid-state diffusion. The containment of the internal gases indicated that the coatings were impermeable. Hence, the apparent success of this batch was real and cannot be attributed to pressure-vessel relief from permeable coatings.

The micropore distribution up to about 10 nm for four of the coating batches, determined by SAXS measurements, is shown in Fig. 8. Values of pore volume are compared to those of a standard pyrolytic carbon. Of interest are the relative distributions of the pore volumes and the peaking exhibited by OR-2013-T at around 4.0-nm pore diameter. This contrasts sharply with the other three batches with coating rates of at least 2.9 μm/min and with BAFs below 1.07. Clearly, OR-2013-T is unique

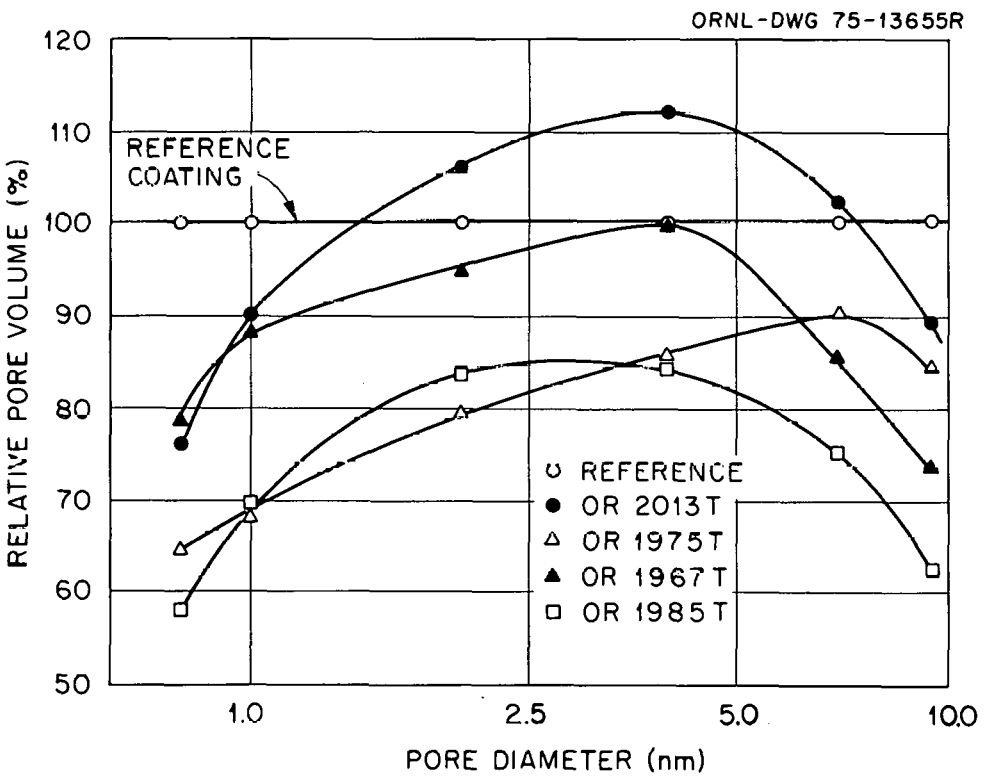

Fig. 8. A comparison of pore volumes of several LTI coatings as measured by small-angle x-ray scattering.

in both microstructure and resistance to radiation-induced failure. It is also unique in that it was fabricated with CO_2-diluted rather than argon-diluted propylene.

CONCLUSIONS

Most coatings used in this series of irradiation tests show that a high deposition rate by itself does not assure a stable coating. While these coatings, produced in a 0.025-m (1-in.) coater, cannot be considered representative of coatings deposited at similar rates in large coaters, it is very important to acknowledge that deposition rate alone is not an adequate criterion for stability. This shows the importance of characterizing coatings on the basis of measurable properties and of identifying those properties that determine irradiation performance. Therefore, work should continue to characterize pyrocarbon coatings to improve our understanding of why some coatings failed despite high deposition rates and relatively low BAF values. Future experiments have been planned to consider process specifications, including hydrocarbon type, diluent, and concentration, as well as coating rate.

The major points shown by these experiments may be summarized as follows:

1. Use of CO_2 rather than argon diluent in the coating gas resulted in a more stable coating in the one specimen tested. The reason for this is not yet clear.
2. Low anisotropy values alone do not assure the stability of dense pyrocarbons under fast-neutron irradiation.
3. The coatings tested in this experiment may have been too dense for optimum irradiation stability.
4. Large density gradients must be also considered, as absolute density values and other factors are, in judging detrimental effects on performance.
5. Biso coatings on dense thoria kernels as large as 680 μm have yet to perform adequately.

6. The process specification, high deposition rate, alone does not guarantee the stability of dense pyrocarbon coatings.
7. Irradiation stability appears to relate strongly to the amount of the fibrous component in pyrocarbon, as determined by SAXS.
8. Further development of product characterization techniques is needed to qualify pyrocarbon coatings for irradiation stability.

ACKNOWLEDGMENTS

The authors wish to acknowledge the efforts of many people who made significant contributions to the planning, execution, and evaluation of this experiment. W. H. Montgomery and J. A. Conlin of the Engineering Technology Division participated in the planning, design, and construction of this series of capsules. C. Hamby, Jr., and W. J. Lackey of the Metals and Ceramics Division assisted in producing the pyrolytic carbon coatings, and H. Keating assisted in coating characterization. Metallography and radiography of the unirradiated particles were done by M. D. Allen and W. J. Mason, respectively, of the Metals and Ceramics Division. The ORNL OPTAF measurements were performed by E. S. Bomar of the Metals and Ceramics Division and the small-angle x-ray scattering measurements were provided by P. Krautwasser of the Institut für Reaktorwerkstoffe der Kernforschungsanlage Jülich, GmbH. The postirradiation fission product inventory measurements were provided by T. B. Lindemer of the Chemical Technology Division. The authors also wish to express thanks to our reviewers E. S. Bomar and P. Angelini of the Metals and Ceramics Division for their helpful comments and questions and acknowledge the assistance of those who helped prepare this report — Nan Richards and Bill McCauley for technical editing; Mary Ellen Smith, Kathy Craft, and Sandi Lyttle for Word Processing; and Ginger Turpin for makeup.

REFERENCES

1. C. B. Scott and D. P. Harmon, *Evaluation of Coated Thorium Oxide Fuel Particles Irradiated in HT-12 through HT-15 and HT-17 through HT-19*, GA-A-13557 (October 1977).

2. M. J. Kania et al., *Irradiation Performance of HTGR Fertile Fuel in HFIR Target Capsules HT-12 through HT-15: Part 1 — Experiment Description and Fission Product Behavior*, ORNL/TM-5305 (February 1977).

3. R. L. Beatty, "Oxidizing Diluent for Fluidized-Bed Pyrolytic Carbon Deposition," *Bull. Amer. Ceram. Soc.* 52(9): 720 (September 1973).

4. G. Tassone, "Bacon Anisotropy Factor Measurements on PYC by X-Ray Diffractomy," *Carbon* 8: 387-88 (June 1970).

5. E. S. Bomar and W. P. Eatherly, "Optical Anisotropy (OPTAF) Measurements," *Gas-Cooled Reactor Program. Annu. Prog. Rep., Dec. 31, 1972*, ORNL-4911, pp. 83-84.

6. C. S. Morgan, W. P. Eatherly, and G. L. Powell, "Inert Gas Permeability of Pyrocarbon Coatings," pp. 111-12 in *13th Bienn. Conf. Carbon, Extended Abstracts and Program* (July 18-22, 1977, Irvine, Calif.).

7. P. Krautwasser, *About the Microporosity of Pyrocarbon Coatings Determined by X-Ray Measurements*, Jül-1202 (May 1975).

8. P. Krautwasser et al., "Comparison of Pyrolytic Carbon Microstructures Derived from MAPP-Gas and Propylene," in *Proceedings of the 6th International Materials Symposium: Ceramic Microstructures '76*, University of California, Berkeley, 1976.

9. M. J. Kania, T. B. Lindemer, M. T. Morgan, and J M Robbins, *Irradiation Performance of HTGR Fertile Fuel in HFIR Target Capsules HT-12 through HT-15*, ORNL/TM-5305 (February 1977).

10. B. H. Montgomery, "HFIR Irradiations, Target Irradiation Tests," *Thorium Utilization Program. Annu. Prog. Rep. Sept. 30, 1971*, ORNL-4760, pp. 134-36.

11. M. J. Kania, *HTCAP — A FORTRAN IV Program for Calculating Coated Particle Operating Temperatures in HFIR Target Irradiation Experiments*, ORNL/TM-5332 (May 1976).

12. B. H. Montgomery, Engineering Technology Div., ORNL, personal communication.

Appendix A

PRE- AND POSTIRRADIATION DIMENSIONS OF GRAPHITE COMPONENTS OF HT-19

THIS PAGE

WAS INTENTIONALLY

LEFT BLANK

Table A-1. Dimensional changes for the high- and low-temperature graphite magazines for HT-19

Magazine	Outside diameter (mm)						Inside diameter (mm)		Length (mm)	
	Large		Midpoint		Small					
	0°	90°	0°	90°	0°	90°	0°	90°	0°	90°
					Preirradiation[a]					
CP-72, -75	13.053	13.028	*b*		12.727	12.702	9.855	9.804	10.949	10.944
CP-73, -74	12.611	12.585	*b*		12.103	12.077	9.855	9.804	10.949	10.944
					Postirradiation					
CP-72	13.108	13.136	13.012	13.030	12.801	12.829	*b*		*b*	
CP-73	12.816	12.829	12.534	12.506	12.141	12.161	*b*		*b*	
CP-74	*b*		*b*		*b*		*b*		*b*	
CP-75	13.020	13.088	13.002	13.020	12.849	12.857	*b*		*b*	

[a]Preirradiation dimensions are the same as design dimensions.

[b]Dimensions were not measured.

Table A-2. Diameter changes for graphite crucibles in HT-19

Holder	Diameter (mm)	Change (percent)[a]
2	9.896	1.2
4	9.893	1.2
5	[b]	[b]
7	9.944	1.7
8	[b]	[b]
10	9.919	1.4
11	[b]	[b]
13	9.921	1.5
15	10.193	4.2
17	[b]	[b]
18	10.071	3.0
20	10.121	3.5
21	[b]	[b]
23	10.096	3.2
24	[b]	[b]
26	[b]	[b]
27	[b]	[b]
29	[b]	[b]
30	[b]	[b]
32	[b]	[b]
33	[b]	[b]
35	[b]	[b]
36	[b]	[b]
38	[b]	[b]
40	9.888	1.1
42	9.881	1.0
43	[b]	[b]
45	9.901	1.2
46	[b]	[b]
48	9.926	1.5
49	[b]	[b]
51	9.916	1.4

[a] Percent change based on a preirradiation design diameter of 9.779 mm.

[b] Diameters were not measured.

Appendix B

THERMAL ANALYSES OF HFIR IRRADIATION CAPSULES HT-17, -18, AND -19

THIS PAGE

WAS INTENTIONALLY

LEFT BLANK

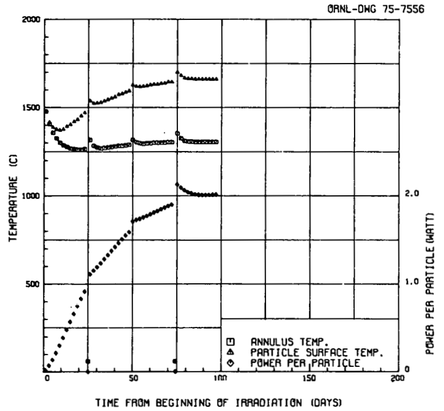

Batch OR-2010-T, Holder 15 (HT-17 and -18)

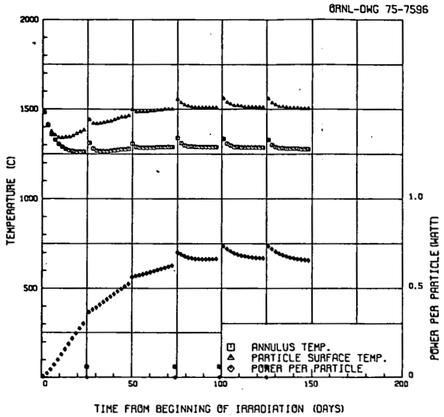

Batch OR-1975-T, Holder 15 (HT-19)

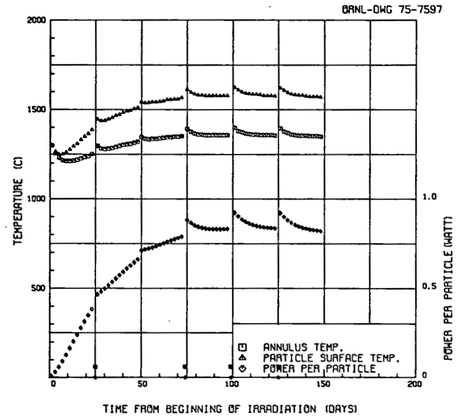

Batch OR-2012-ST, Holder 17

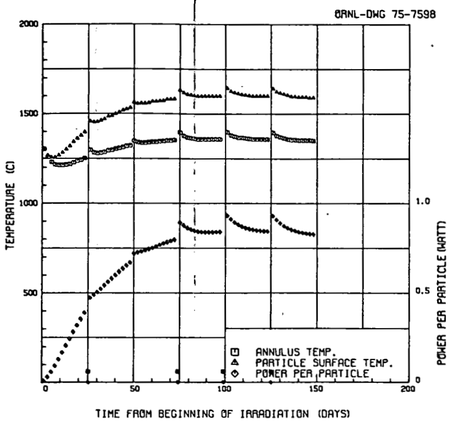

Batch OR-1987-T, Holder 18

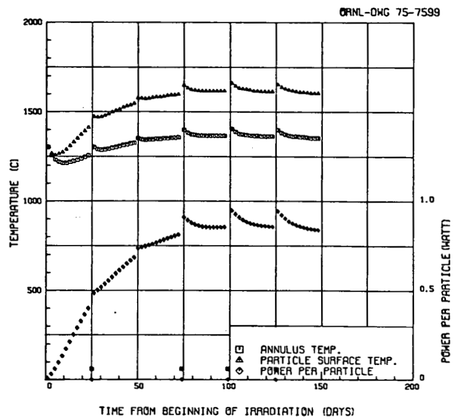

Batch OR-1972-T, Holder 20

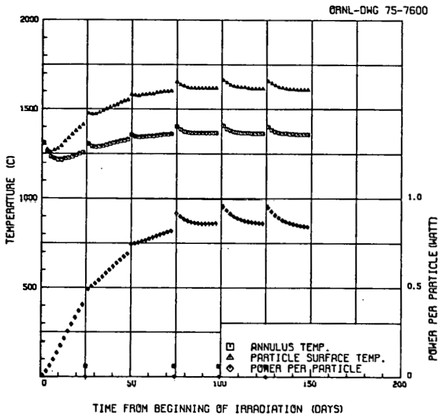

Batch OR-1986-T, Holder 21

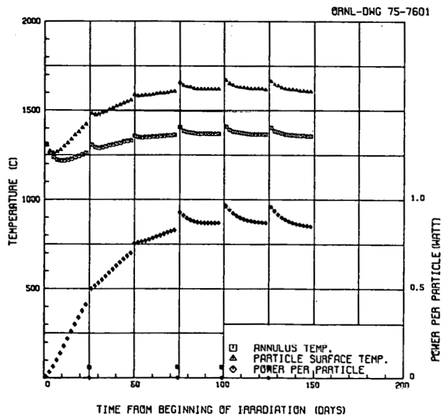

Batch OR-1985-T, Holder 23

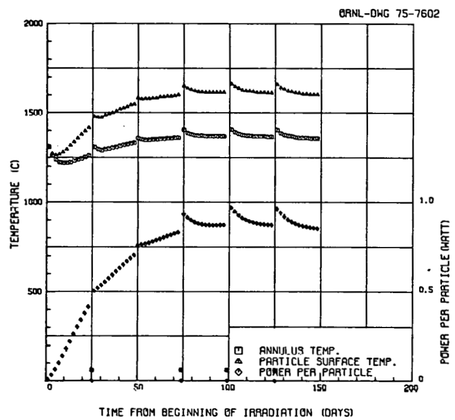

Batch OR-1967-T, Holder 24

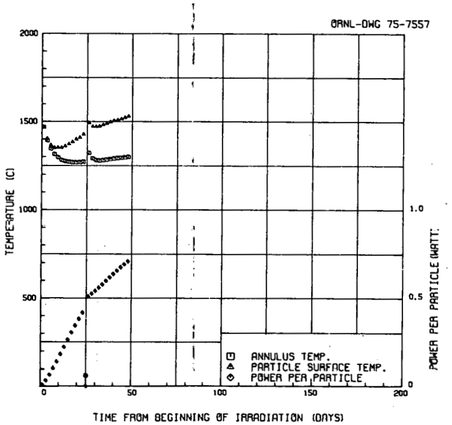

Batch OR-1978-T, Holder 26 (HT-17)

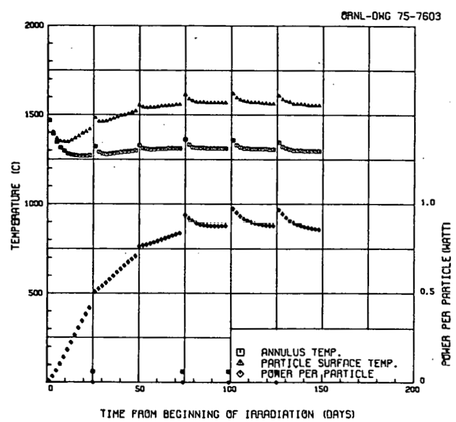

Batch OR-2013-T, Holder 26 (HT-18 and -19)

Fig. B.1. Temperature and power histories for ORNL Biso-ThO_2 particles during irradiation in the high-temperature magazines from capsules HT-17, -18, and -19.

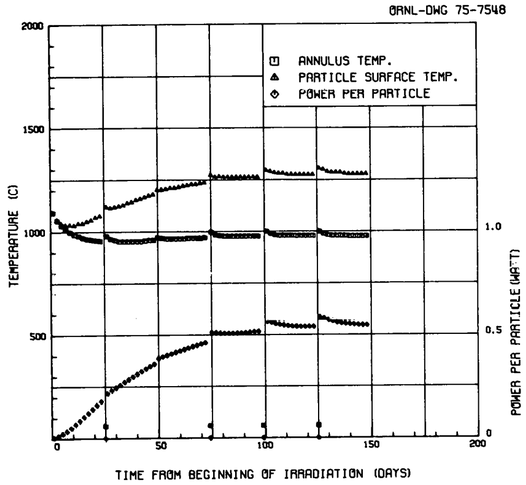

Batch OR-1978-T, Holder 2

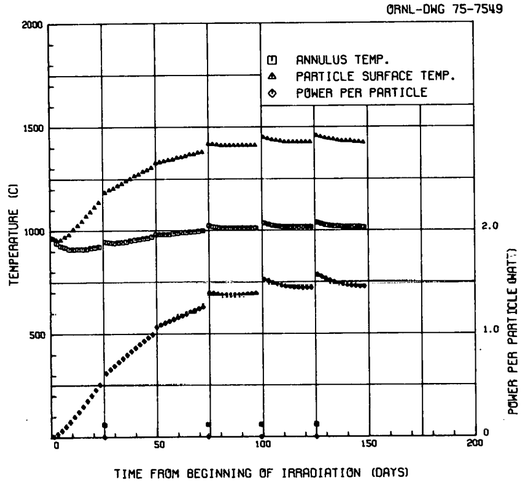

Batch OR-2010-T, Holder 4

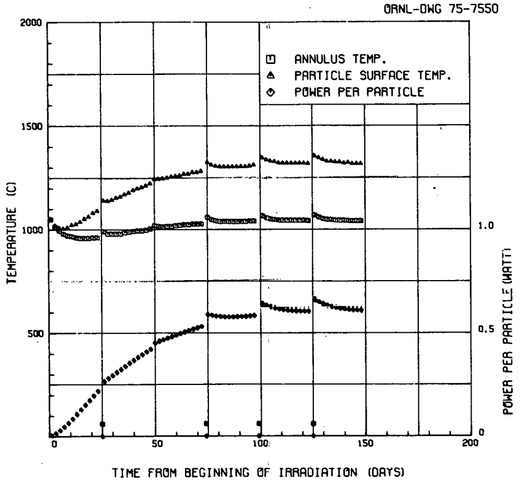

Batch OR-2012-ST, Holder 5

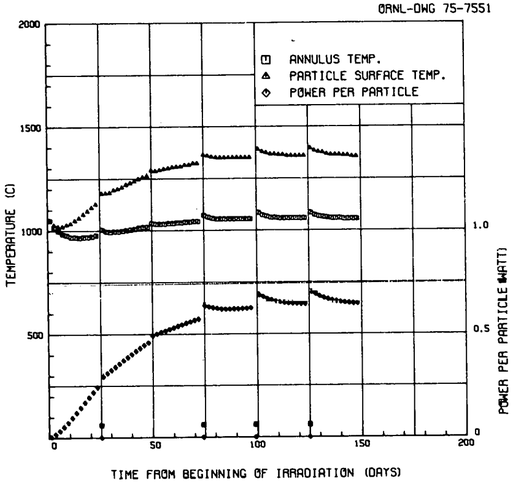

Batch OR-1987-T, Holder 7

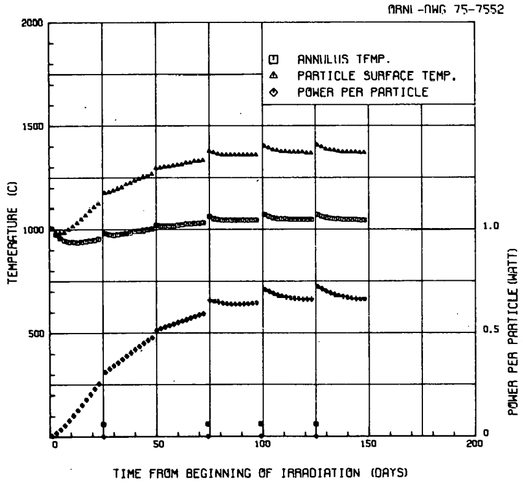

Batch OR-1972-T, Holder 8

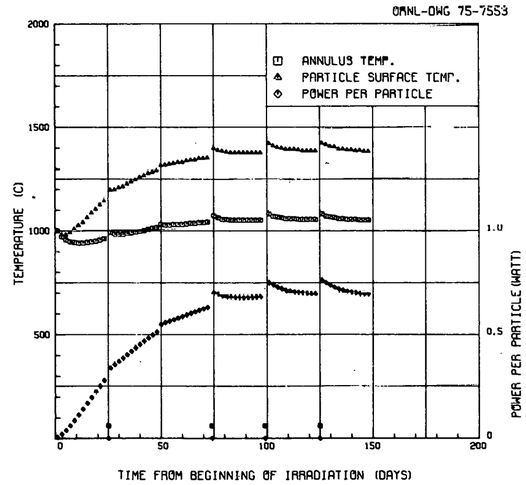

Batch OR-1986-T, Holder 10

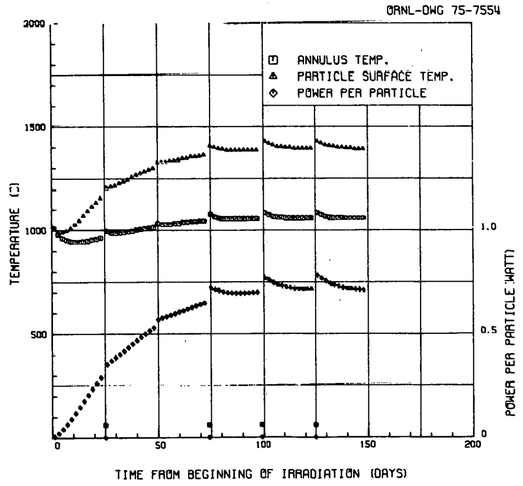

Batch OR-1985-T, Holder 11

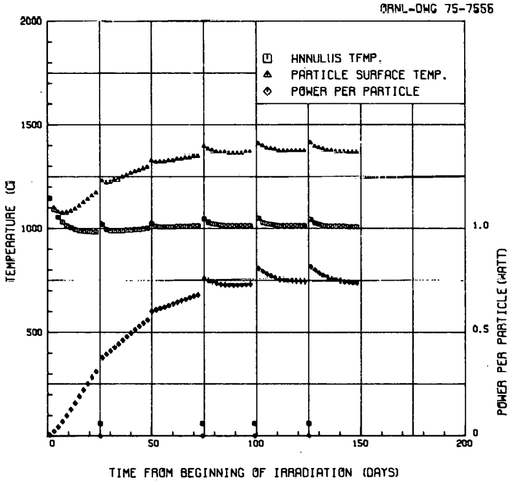

Batch OR-1967-T, Holder 13

Fig. B-2. Temperature and power histories for ORNL Biso-ThO_2 particles during irradiation in the low-temperature magazines from capsules HT-17, -18, and -19.

ORNL/TM-6414
Dist. Category UC-77

INTERNAL DISTRIBUTION

1-2. Central Research Library
3. Document Reference Section
4-6. Laboratory Records Department
7. Laboratory Records, ORNL RC
8. ORNL Patent Office
9-11. Technical Publications Department
12. P. Angelini
13-17. R. L. Beatty
18. B. J. Bolfing
19. R. A. Bradley
20. A. J. Caputo
21. D. A. Costanzo
22. R. S. Crouse
23-27. W. P. Eatherly
28. R. J. Gray
29. R. E. Helms
30-32. M. R. Hill
33. F. J. Homan
34. J. A. Horak
35-39. M. J. Kania
40-49. P. R. Kasten
50. W. J. Lackey
51. K. H. Lin
52. T. B. Lindemer
53-62. E. L. Long, Jr.
63. A. L. Lotts
64. J. E. Mack
65. W. R. McCauley
66. C. S. Morgan
67. A. R. Olsen
68. M. F. Osborne
69. R. L. Pearson
70. H. Postma
71-75. J. M. Robbins
76. J. E. Selle
77. R. L. Senne
78. C. J. Sparks, Jr.
79. D. P. Stinton
80. V. J. Tennery
81. S. M. Tiegs
82. T. N. Tiegs
83. D. R. Vondy
84. G. W. Weber
85. R. W. Balluffi (consultant)
86. P. M. Brister (consultant)
87. W. R. Hibbard (consultant)
88. M. J. Mayfield (consultant)
89. N. E. Promisel (consultant)
90. J. T. Stringer (consultant)

EXTERNAL DISTRIBUTION

91-94. DOE Division of Nuclear Power Development, Washington, DC 20545

Director
Assistant Director, Fuel Cycle
Chief, Technology Branch
Chief, Projects Branch

95. DOE Idaho Operations Office, P.O. Box 2108, Idaho Falls, ID 83401

Barry Smith

96. San-Development, San Diego Area Office, P.O. Box 81325, San Diego, CA 92138

Senior Program Coordinator

97. DOE Oak Ridge Operations Office, P.O. Box E, Oak Ridge, TN 37830

Director, Research and Technical Support Division

98-274. DOE Technical Information Center, P.O. Box 62, Oak Ridge, TN 37830

For distribution as shown in TID-4500 Distribution Category, UC-77 (Gas-Cooled Reactor Technology)

☆ U.S. GOVERNMENT PRINTING OFFICE: 1977-748-189/274